Electrophoretic Mobilities of RNA Tumor Viruses. Studies by Doppler-Shifted Light Scattering Spectroscopy†

Lajos Rimai,* Irving Salmeen, David Hart, Leonard Liebes, Marvin A. Rich, and J. Justin McCormick

ABSTRACT: We have used laser beat frequency light scattering spectroscopy to measure, at several pH values, the electrophoretic mobilities of purified avian myeloblastosis (AMV), murine leukemia (MuLV), murine mammary tumor (MuMTV), and feline leukemia (FeLV) viruses. The mobilities of these viruses are similar at pH ≥ 7 (-2.7 to -3.2×10^{-4} (cm/sec)/(V/cm)). The isoelectric points of MuLV and AMV are apparently less than pH 3, whereas for FeLV the data could be interpreted to indicate an isoelectric point between 3 and 5. Using a Debye-Hückel model to describe the interaction between electrolytes and virus, we show that our values for the mobility of MuMTV, obtained in ionic strength 0.005, are consistent with the values of Sarkar et al. ((1973), *Cancer Res. 33,* 2283), obtained in ionic strength of 0.10. This model is then used to calculate surface charge densities. In terms of the density of charged groups, the RNA tumor virus envelope is not very different from the erythrocyte membrane.

Various RNA tumor viruses have been extensively studied by electron microscopy (Bader, 1969; Luftig et al., 1974; Luftig and Kilham, 1971). Physical studies of these viruses in solution have been concerned almost exclusively with determinations of buoyant densities and sedimentation coefficients (Manning et al., 1970; Sharp and Beard, 1954; Mora et al., 1966). Recently we have used laser beat frequency spectroscopy (LBFS[1]) (also called quasielastic scattering, intensity fluctuation spectroscopy, and optical mixing spectroscopy) to measure the diffusion constants and hydrodynamic diameters of avian myeloblastosis virus (AMV) and murine leukemia virus (MuLV, Rauscher) under identical solution conditions (Salmeen et al., 1975). In this paper we report measurements by LBFS of electrophoretic mobilities for several RNA tumor viruses, including murine mammary tumor virus (MuMTV). The only previous electrophoresis study of these viruses was carried out on MuMTV by conventional moving boundary electrophoresis (Moore and Lyons, 1963, Sarkar et al., 1973).

The measurement of electrophoretic mobilities by LBFS is based on the fact that light scattered by particles moving uniformly is shifted in frequency by an amount proportional to the particle velocity (the doppler shift). This technique was first used by Ware and Flygare (1971) to measure mobilities of some proteins, and later by Uzgiris (Uzgiris, 1972; Uzgiris and Kaplan, 1974) to measure mobilities of bacteria, erythrocytes, and lymphocytes. This technique enables the measurement of oncornavirus mobilities at concentrations as low as 10^7 particles/ml with an accuracy of ±5%. The total measurement time is in the order of minutes. We have measured the mobilities of purified samples of AMV, MuLV, feline leukemia virus (FeLV), and MuMTV over a range of pH values. Using a Debye-Hückel model (Tanford, 1961; Henry, 1931; Booth, 1950) to describe the interaction between electrolytes and virus, we show that our values for the mobility of MuMTV, obtained in low ionic strength buffer ($I = 0.005$), are consistent with the values reported by Sarkar et al. (1973), obtained in high ionic strength buffer ($I = 0.10$). This model is then used to calculate the surface charge densities of the virions. These are found to be within 30% of the charge densities of human erythrocytes and within a factor of 2 of that of cultured hamster fibroblasts (Ambrose, 1966; Heard and Seaman; 1960).

Summary of Basic Concepts

The basic theory of LBFS has been reviewed in a number of recent publications (Rimai et al., 1970; Clark et al., 1970; Pusey et al., 1974). In this section, we summarize those concepts and relationships that are necessary for understanding the method and the data analysis.

The scattered light is detected with a photomultiplier tube and the photocurrent is analyzed in terms of either its frequency power spectrum or its time autocorrelation function. The photocurrent is proportional to the integral, over the photocathode surface, of the scattered radiation power density incident on the photocathode. At a given point, R, of the photocathode, this power density is proportional to the square of the total scattered electric field at R:

$$P(R) = \sum_i E_i^2(R) + \sum_i \sum_{j \neq i} E_i(R) E_j(R) \cos \Phi_{ij} \quad (1)$$

$E_i(R)$ and $E_j(R)$ are the scattered field intensities originating from particles i and j (at locations r_i and r_j with respect to the center of the photocathode). Isotropic scattering of linearly polarized incident radiation is assumed so that the scattered fields can be expressed by scalar quantities. Φ_{ij} are the phase differences, due to propagation time differences, between the fields radiated from i and j, when the two scattered waves reach the point R. For identical scatterers and for particle concentrations sufficiently large that total particle number fluctuations in the scattering volume

† From the Scientific Research Staff, Ford Motor Company, Dearborn, Michigan 48121 (L.R., I.S., and D.H.), and the Michigan Cancer Foundation, Detroit, Michigan 48201 (L.L., M.A.R., and J.J. McC.). *Received May 9, 1975.* This research was supported by NCI Contract N01-CP-33226, and Grants CA 13058 and CA 14060, and by an institutional grant from the United Foundation of Greater Detroit.

[1] Abbreviations used are: LBFS, laser beat frequency spectroscopy; AMV, avian myeloblastosis virus; FeLV, feline leukemia virus; MuLV, mouse leukemia virus; MuMTV, mouse mammary tumor virus.

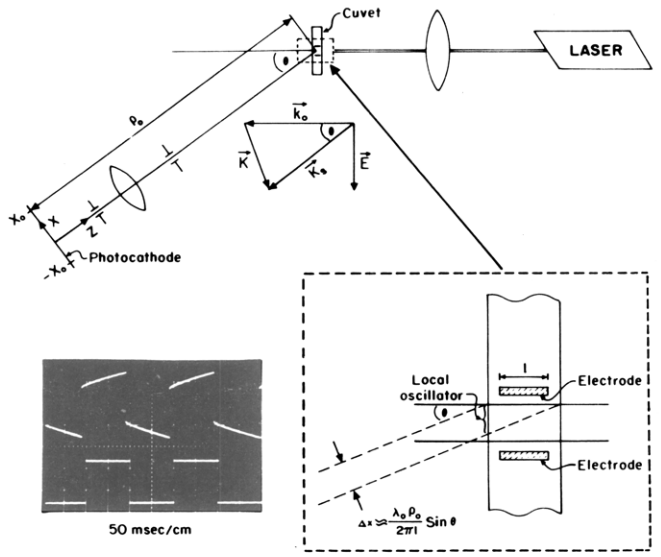

FIGURE 1: Schematic of the optical system for electrophoretic light scattering (symbols defined in text). Inset: details of geometry of the scattering volume involved in defining the coherence volume. Top and bottom oscilloscope traces are respectively the voltage across and the current through the electrodes. Time scale, 50 msec/large division; vertical scale, 0.5 V/large division in upper trace, 20 V/large division in lower trace. The current waveform is obtained as the voltage drop across a 50-kΩ resistor in series with the electrodes. The initial sharp rise in voltage corresponds to the ir drop across the solution.

may be neglected, the first term of eq 1 is a constant which is proportional to the total number of particles in the scattering volume. The second term is time dependent and reflects fluctuating interferences due to changes in Φ_{ij} brought about by the relative motion of the particles. If there are no refraction effects at the boundary of the solvent then:

$$\Phi_{ij} = (\mathbf{k} - \mathbf{k}_0) \cdot (\mathbf{r}_i - \mathbf{r}_j) = \mathbf{K} \cdot (\mathbf{r}_i - \mathbf{r}_j) \qquad (2)$$

where $\mathbf{k}_0$ and $\mathbf{k}$ are the wave vectors respectively of the incident and scattered radiation. For these experiments $|\mathbf{k}| \simeq |\mathbf{k}_0| = 2\pi n/\lambda_0$, where n is the solvent refractive index, λ_0 the vacuum wavelength of the incident light, and $|\mathbf{K}| \simeq 2|\mathbf{k}_0| \sin(\theta/2)$, where θ is the (internal) scattering angle. The only terms of the interference double sum which contribute to the integral of $P(R)$ over the finite area of the photocathode are those for which $|\mathbf{r}_i - \mathbf{r}_j|$ is sufficiently small so that cos Φ_{ij} does not oscillate as R moves over the photocathode. More specifically, let (x_i, y_i, z_i) be the rectangular components of $\mathbf{r}_i$ in a coordinate system with origin on the photocathode, z normal to the photocathode directed toward the center of the scattering volume, and x in the scattering plane. Let (XY) be the coordinates of R and let the photocathode extend from $-X_0$ to X_0 and $-Y_0$ to Y_0 (see Figure 1). Then, in order for the scattering from two particles i and j to contribute to the interference term the following inequalities hold:

$$(x_i - x_j) < \frac{m\lambda_0\rho_0}{2\pi X_0}$$

and

$$(y_i - y_j) < \frac{m\lambda_0\rho_0}{2\pi Y_0} \qquad (3)$$

ρ_0 is the distance between the centers of the photocathode and scattering volume, and $\pi/2 < m < \pi$. The z-coordinate difference is arbitrary since the z direction is normal to the photocathode. Thus, the double sum in eq 1 extends only over those pairs of scatterers which are sufficiently close to each other so that eq 3 is satisfied. Such pairs are said to be within one coherence volume (Clark et al., 1970). The ratios ρ_0/X_0 and ρ_0/Y_0 define the receiver aperture F numbers, F_x and F_y (Born and Wolf, 1964). For isotropic scattering of light polarized in the y direction, the effective aperture $(1/F_y)$ in the y direction is determined not by the receiver optics, but by the fact that the scattered intensity drops rapidly as the scattering direction moves out of the x–z plane. Thus no matter how large the actual numerical aperture of the receiver optics, the effective aperture is very small and only the inequality in x imposes limitations on the receiver optics.

It can be shown that for scattering from identical particles undergoing only Brownian motion, the photocurrent time autocorrelation function and its frequency power spectrum respectively are of the forms:

$$\langle I(\tau)I(\tau + t)\rangle = Ae^{-2DK^2t}$$

$$I_p(\nu) = \frac{A2DK^2}{4\pi^2\nu^2 + (2DK^2)^2}$$

where D is the particle diffusion constant (Rimai et al., 1970; Clark et al., 1970). In this case, uniform flow of velocity V would not be reflected in the time fluctuations of $I(t)$ because the phase *differences* are independent of time:

$$\Phi_{ij}(t + \Delta t) = \mathbf{K} \cdot [\mathbf{r}_i + V\Delta t - \mathbf{r}_j - V\Delta t] = \Phi_{ij}(t)$$

In order to detect uniform flow by this method, strong scattering from a stationary "local oscillator" source is introduced, which serves as a phase reference. If, in eq 1, the scattering from a stationary point, say $i = 0$, is sufficiently strong, then the double sum is dominated by terms with $i = 0$, and, when all suspended particles undergo uniform motion of velocity V, the phase differences with respect to the stationary source will depend linearly on time:

$$\Phi_{0j} = \mathbf{K} \cdot (\mathbf{r}_0 - \mathbf{r}_j) + \mathbf{K} \cdot Vt$$

Under these conditions, the time dependence of the photocurrent will reflect the presence of the flow through the doppler shift $\delta\nu = \mathbf{K} \cdot V/2\pi$. The only scattering particles which contribute to the double sum are those within the coherence volume surrounding the local oscillator. In this case, the current correlation function and power spectrum have the respective forms:

$$\langle I(\tau)I(\tau + t)\rangle = Ae^{-DK^2t} \cos(2\pi\delta\nu t)$$

$$I_p(\nu) = \frac{ADK^2}{4\pi(\nu - \delta\nu)^2 + (DK^2)^2} \qquad (4)$$

(Bennett and Uzgiris, 1973). The power spectrum, which is the measured function in these experiments, has a peak at the doppler frequency $\delta\nu$, with half-width DK^2.

In the present experiments, V is caused by an electric field, E, applied in the scattering plane, normally to the incident beam, by a pair of platinum electrodes, as indicated in Figure 1. Then $V = \mu E$ where μ is the electrophoretic mobility of the particles. The local oscillator may be taken as the elastic scattering from the point at which the incident laser beam either enters or exits the cuvet. In either case, for a substantial fraction of the volume between the electrodes to be contained within the coherence volume of the local oscillator, we require that:

$$l \simeq \frac{m\lambda_0\rho_0}{2\pi X_0 \sin\theta} \quad (5)$$

where l is the electrode dimension parallel to the incident beam. For $l \simeq 0.15$ cm, $\theta \simeq 10°$ and $\lambda_0 = 633$ nm, a receiver aperture corresponding to $F_x \approx 500$ satisfies the condition of eq 5. From the relations developed above and the geometric optics of scattering through the front surface of the cuvet, the doppler shift due to drift velocity V perpendicular to $\mathbf{k}_0$ is given by $\delta\nu = (V/\lambda_0) \sin\theta_0$, where θ_0 is the external scattering angle.

Materials and Methods

Light Scattering Instrument. The experimental arrangement is shown schematically in Figure 1. The sample is contained in a 2 × 10 mm cuvet into which is inserted a pair of parallel plate platinized platinum electrodes (prepared in the manner described by Uzgiris (1974)). Light from a Spectra-Physics Model 125 He-Ne laser (nominally 50 mW at 632.8 nm) is focused by a lens through a 10-mm face into the sample volume between the electrodes. The scattered light is collected through the other 10-mm face at external scattering angles between 10 and 30° and imaged through lenses and slits onto the photocathode of a photomultiplier tube. The slits determine an F number which ensures that the conditions of eq 3 and 5 are met for effective mixing with the local oscillator, which is supplied by light scattered elastically from the cuvet wall at the point where the beam exits. The photocurrent passes through a 100 kΩ load resistor and, after amplification with a Tektronix Model AM-502 amplifier, the corresponding voltage drop is applied to the input of a 200 channel Saicor Real Time spectrum analyzer. The spectrum analyzer could be replaced by a correlator; however, the damped oscillating correlation function is more difficult to analyze than the power spectrum, especially in the presence of multiple frequencies. In addition, the live time spectral display offered by the harmonic analyzer facilitates optimization and system alignment.

Uzgiris (1974) has discussed the requirements of the electrode design and the advantages of platinized platinum electrodes over other types. We use electrodes about 1.5 mm wide and 4 mm high, machined from 0.33 mm thick platinum stock and welded to no. 30 platinum wires. Data were obtained with electrode spacings which varied between 0.25 and 1.5 mm. The wires extend through a Teflon support which is mounted in a rotatable platform located above the cuvet. For mechanical stability, the part of the platinum wires extending from the Teflon support to the platinum electrode plates are embedded in epoxy. This entire assembly is mounted on a micrometer-adjustable x-y-z stage so that the electrodes can be moved not only in and out of the sample, but also perpendicularly to the incident beam.

In order to minimize bubbling caused by gas evolution at the electrodes, and in order to avoid irreversible electrode polarization, the current is applied to the electrodes in short pulses of alternating polarity. The electric field actually applied to the sample is given by the linear resistive voltage drop across the sample divided by the electrode spacing. The electrodes add nonlinear resistances because of electrode polarization effects, and capacitances because of double layer build up. Therefore, in order to ensure a constant field in the sample, and hence a constant doppler shift, the electrodes need to be driven by a constant current source. This is achieved by using a large series resistor between the voltage source and the electrodes. The electrodes and series resistor are connected between the emitters of two power transistors gated by alternating pulses so that each pulse reverses the sign of the applied voltage. The current is applied in bursts of a few seconds duration with 10–20 pulses/burst. The spectrum analyzer is gated-on synchronously with each burst so that data are accumulated only while the field is on. A period of several seconds is allowed to lapse between bursts in order to minimize joule heating of the sample. The voltage wave form across the electrodes is shown in Figure 1. The voltage attained after the initial fast rise corresponds to the ir(resistive) drop across the sample, whereas the subsequent slower rising portion corresponds to additive effects at the electrodes.

The temperature of the sample is determined mainly by ambient room temperature, and is monitored with a thermistor in good thermal contact with the cuvet. Sample temperatures were between 24 and 26°C and were constant to within ±0.1°C during the time of one measurement.

The sign of the mobility can be determined directly on high concentration samples by observing the direction of motion of the scattered light projected on a screen (Uzgiris and Costaschuk, 1973). As noted in the Results section, some samples have a scattered intensity too weak for direct observation of the sign.

The precision of the measurements for a given virus at a given pH is indicated by the error limits in Table I. These are root mean square (rms) deviations, calculated for a minimum of two independently purified samples, for various electrode spacings, and for different applied field values. For each case, at least ten independent measurements have been included. Where measurements are repeated for the same sample at the same applied field (i.e., the precision of the spectral measurements themselves) the rms deviation is always less than $\pm 0.03 \times 10^{-4}$ (cm/sec)/(V/cm).

Sample Preparation. AMV (BAI strain) in plasma citrate was supplied by Drs. Joseph and Dorothy Beard; MuLV (Rauscher) in plasma citrate was supplied by University Laboratories; concentrated FeLV, derived from cell line FL-74, was supplied by Pfizer Inc., Maywood, N.J.; RIII milk containing MuMTV was supplied by Meloy Laboratories, Arlington, Va. All of these viruses were obtained through the cooperation of the Virus Cancer Program of the National Cancer Institute.

The MuLV, AMV, and FeLV preparations were purified by the sucrose density gradient purification treatments described previously (Salmeen et al., 1975). MuMTV was purified from RIII milk by a procedure adapted from that described by Lyons and Moore (1965) and Manning et al. (1970); 4 ml of mouse milk was pooled and mixed with an equal volume of 0.15 M EDTA (pH 7.0). The skim milk was separated from the lipid (cream) by two low speed centrifugations (1465g, 15 min and 10,400g, 10 min, 4°C). The lipid was discarded after each of these centrifugations and the remaining supernatant was centrifuged for 1 hr (Spinco SW 50.1 rotor, 139,000g) on a discontinuous 20–65% w/w sucrose gradient prepared in 0.005 ionic strength NaH_2PO_4–K_2HPO_4 (pH 7.0) buffer. The virus was removed from the pad and centrifuged isopycnically in a 20–65% w/w continuous sucrose gradient (Spinco SW 41, 206,000g, 3 hr). Virus bands were removed from the sucrose gradients with an illuminated tube piercing apparatus (Schaffer and Fromhagen, 1965). The samples were then dialyzed against three changes of the appropriate buffer.

Table 1: Electrophoretic Data on RNA Tumor Viruses.

Particle	pH	Radius[b] ($R \times 10^7$) cm	Mobility ($\mu \times 10^4$) (cm/sec)/(V/cm)	Surface Charge Density[c] ($\sigma_\infty \times 10^{-3}$) esu	($\sigma \times 10^{-3}$) esu	Total Charge ($4\pi R^2 \sigma \times 10^6$) esu
MuLV[a]	9	72	2.8 ± 0.1	1.74	2.16	1.41
	7	72	2.7 ± 0.1	1.92	2.39	1.56
	5	80	1.65 ± 0.1	1.04	1.24	0.84
	3		1.02 ± 0.1			
AMV[a]	9	72	2.64 ± 0.1	1.64	2.04	1.33
	7	73	2.78 ± 0.2	1.72	2.13	1.43
	5	75	1.84 ± 0.05	1.14	1.40	0.99
	3		1.63 ± 0.05			
FeLV[a]	9	86	3.19 ± 0.2	1.98	2.26	2.10
	7	86	2.71 ± 0.1	1.68	1.91	1.77
	5	86	2.20 ± 0.1	1.37	1.56	1.45
	3		2.60 ± 0.2			
MuMTV[a]	9	72	3.01 ± 0.2	1.87	2.32	1.51
	7	72	2.68 ± 0.2	1.66	2.07	1.38
	5	72	2.36 ± 0.2	1.46	1.83	1.26
Erythrocytes (0.28 *M* sucrose)	7		3.13 ± 0.05	2.48		
Hamster Fibroblasts[d] ($I = 0.15$)	7		1.0	3.3		
Hamster Fibroblasts Transformed[d]	7		1.2	3.9		

[a] In 0.005 ionic strength buffer unless otherwise indicated. [b] Determined by LBFS. [c] See eq 7 and 7a in text. [d] Ambrose, 1966.

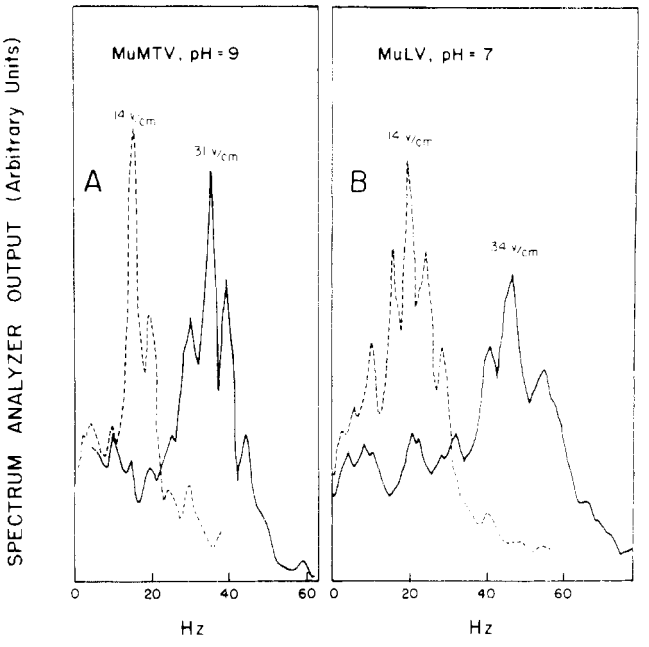

FIGURE 2: Examples of electrophoretic light scattering power spectra for two RNA tumor viruses. (A) MuMTV, pH 9, ionic strength, I = 0.005; approximate concentration, 10^8 particles/ml; T = 25°C; external scattering angle, 15°; electrode spacing 0.64 mm. Total data accumulation time, approximately 1 min. The applied electric fields are indicated at the peaks. (B) MuLV, pH 7, other conditions are the same as in A. The sideband structure is a result of the fact that the pulse alternation rate is not completely negligible compared to the doppler shift (Uzgiris and Costaschuk, 1971).

The last change contained 0.02% (w/v) sodium azide.

For virus samples in different pH buffers, the virus preparations were pooled, and aliquots were removed, purified by centrifugation, and dialyzed into appropriate buffers of 0.005 ionic strength. The buffers were prepared according to the tables found in the Biochemists' Handbook (Long, 1961). The respective buffers were: pH 3, glycine-HCl-glycine; pH 5, acetic acid-sodium acetate; pH 7, KH_2PO_4-Na_2HPO_4; and pH 9, $NaHCO_3$-Na_2CO_3.

The erythrocyte test sample was prepared from whole blood (human) which was collected with heparin-treated equipment. The cells were first washed exhaustively using a pH 7.4 isotonic phosphate buffer (Dodge et al., 1963) and then washed with the 0.005 ionic strength, pH 7.0 phosphate buffer made isotonic with the addition of sucrose (10.8% w/v).

Results

Figure 2A and B show typical spectra for MuMTV and MuLV at two different values of applied field. Instrumental details and sample conditions are given in the figure legend. The spectra have a strong peak at the doppler frequency. Time dependent field inhomogeneities contribute to the line widths which are greater than the expected diffusional width which, at a 11° scattering angle, is ca. 3 Hz. Weak modulation side bands can be discerned in some of the data due to the finite alternation frequency of the applied field (Bennett and Uzgiris, 1973).

Figure 3 contains plots of the doppler shift at a 15° external (11.2° internal) scattering angle as a function of applied field and pH. The pH dependencies of the electrophoretic mobilities are plotted in Figure 4 with data averaged from measurements on several independently prepared samples, obtained at different field values, using various scattering angles and electrode spacings.

The mobilities are negative for samples at pH 5.0 and above, as was expected from electrophoresis studies of cells, other membrane enveloped RNA viruses (Hill et. al., 1972), and MuMTV (Sarkar et al., 1973) using conventional methods. In the present study, the sign of the mobilities could not be measured at pH 3 because the intensity of the

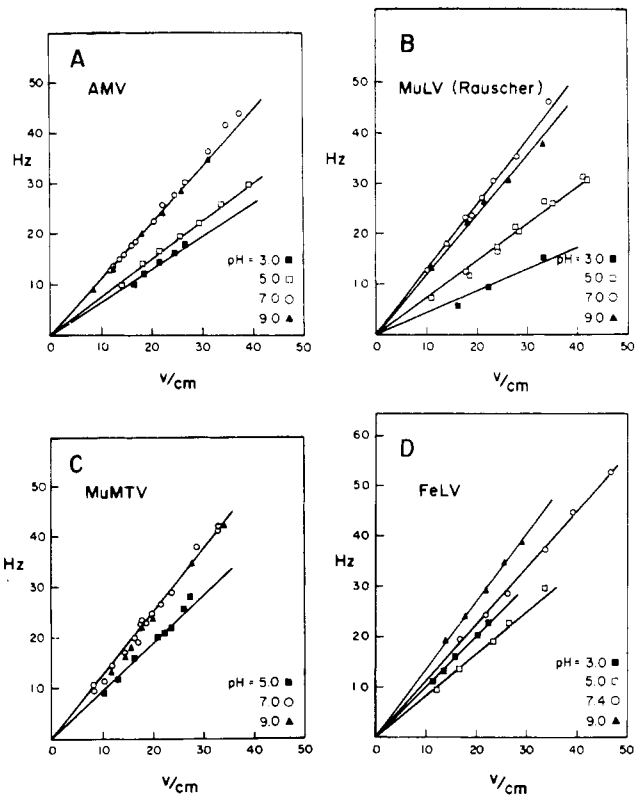

FIGURE 3: Plots of electrophoretic doppler shifts as a function of applied electric fields for the four oncornaviruses obtained in the pH range of 3–9 (I = 0.005, T = 25°C) at an external scattering angle of 15°. Data points represent at least two independent samples for each case and electrode spacings ranging between 0.5 and 1.25 mm. (A) AMV; (B) MuLV; (C) MuMTV; (D) FeLV.

light scattering signal was too weak. This signal weakness is attributed to loss of intact virions at this pH. From published results (Hill et al., 1972; Sarkar et al., 1973), we would expect that the isoelectric point of the oncornaviruses should be less than pH 4. By extrapolation, as shown by the dashed lines in Figure 4, the mobility at pH 3.0 of FeLV could be interpreted as positive thus locating the isoelectric point between pH 3 and pH 5. The isoelectric point of MuLV and AMV could well be less than pH 3. The MuMTV samples showed no significant trace of the virus at pH 3.0, as indicated by the intensity and by the spectrum of the large angle LBFS data, and by the absence of a well-defined electrophoretic peak.

In addition to the studies on the oncornaviruses, we also measured the mobility of human erythrocytes at several ionic strengths. We obtained values which agreed with published measurements, thus verifying our field measurement (see Table I).

Discussion

The simplest expression for the electrophoretic mobility of a particle is $\mu = V/E = q/\beta$ where q is the total charge on the particle and β is its hydrodynamic friction coefficient (Tanford, 1961). Generally, q is an effective charge, since it depends not only on the actual charges on the surface of the virus, but also on the ionic constitution of the suspending medium. This is true even for samples with the very low virus concentrations encountered in these experiments. The friction coefficient is $\beta = 3\pi d\eta$ (Tanford, 1961), where η is the solvent viscosity coefficient and d is the particle diameter. β can be obtained from the diffusion coefficient in the

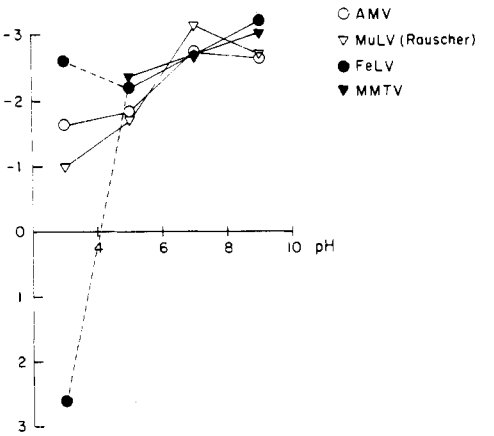

FIGURE 4: Electrophoretic mobilities as a function of pH for the four RNA tumor viruses whose data were presented in Figure 3. The data points are averages for measurements on independent samples, different electrode configurations, and field values. (A minimum of ten independent measurements for each sample.) The error limits are stated in Table I. The absolute sign at pH values ≥5 is negative, and inferred for pH 3. The dashed line refers to the uncertainity in sign for FeLV (see discussion in text).

same solvent since $D = kT/\beta$ (Tanford, 1961). In principle, the electrophoretically shifted spectra yield both D (see eq 4) and μ. However, in practice β is determined best by measuring D with conventional LBFS at much larger angles (e.g., 90°). The hydrodynamic diameters of the viruses were obtained by just such measurements (Salmeen et al., 1975; manuscript in preparation) (see Table I).

In addition to empirically characterizing particles by their electrophoretic mobilities at a given pH, ionic strength, and temperature, these experimental results can yield the surface charge or surface charge density. However, in order to obtain this charge, the data have to be analyzed within the framework of a model that relates, in terms of the solvent electrolyte interactions, the effective charge q, to the real surface charge. Such a model, based on the Poisson–Boltzmann treatment of the potential distribution in the vicinity of a spherical nonconducting particle, has been developed (Tanford, 1961; Henry, 1931; Booth, 1950).

In a first approximation, neglecting effects of the applied field on the electrolyte charge distribution near the particle, this model gives the following expression for the effective particle charge (Tanford, 1961):

$$q = \frac{eZX(\kappa R)}{1 + \kappa R} \tag{6}$$

where e is the charge of one electron, R the particle radius, Z the total charge in units of e, and $\kappa = (8\pi Ne^2 I/1000\epsilon kT)^{1/2}$ is the Debye screening parameter which expresses the dependence of the charge on solvent ionic strength. N is Avogadro's number, ϵ is the solvent dielectric constant, k is the Boltzmann constant, T is the absolute temperature, and I is the ionic strength (mol equiv/l.). The function $X(\kappa R)$ can be obtained directly from Tanford (1961) or indirectly from the data of Booth (1950) and varies between $1 < X(\kappa R) < 1.5$ as κR increases. Equation 6 can be recast in terms of the surface charge density $\sigma = Ze/4\pi R^2$ and the mobility μ:

$$\sigma = \eta\kappa\mu \left\{\frac{1 + \kappa R}{\kappa R} \frac{1.5}{X(\kappa R)}\right\} \tag{7}$$

For $\kappa R \gg 1$, $X(\kappa R) \simeq 1.5$ (Booth, 1950) the surface charge density becomes:

$$\sigma_\infty = \eta\kappa\mu \quad (7a)$$

This expression is independent of particle size. Equation 7a also suggests that even for nonspherical particles, in the limit $\kappa R \gg 1$ (where now R is a typical particle dimension) the mobility becomes independent of shape. Equation 7a is identical with the relation used by Heard and Seaman (1960) to analyze the ionic strength dependence of erythrocyte mobilities, where only the first term in the expansion of the thermal factor is taken into account. (The dependence on ionic strength is not affected by the form of the thermal factor.) This analysis clearly shows that eq 7a is valid when the particle dimensions are larger than 10^{-4} cm for I = 0.005. At pH ≥7, the mobilities of the spherical RNA tumor viruses are essentially pH independent. Thus they can be approximated well by rigid spheres with a time independent charge distribution.

Evidence for the applicability of this model to the particular viruses under study comes from the comparison of our data on MuMTV (pH ≥7) at an ionic strength I = 0.005 (κR = 16.7 for $R = 72 \times 10^{-7}$ cm, as we derived from the diffusion constants, $\mu = 2.65 \times 10^{-4}$-$3.01 \times 10^{-4}$ (cm/sec)/(V/cm) in Table I) with that of Sarkar et al. (1973) at an ionic strength I = 0.1 (κR = 74.5, $\mu = 0.5 \times 10^{-4}$-0.6×10^{-4} (cm/sec)/(V/cm)). Equation 7 predicts $\mu(I = 0.005)/\mu(I = 0.1)$ = 4.63, whereas the experimental ratios range between 6 and 4.4.

Table I shows the mobilities, the surface charge densities (obtained by use of eq 7), and the total charge for the four RNA tumor viruses we have studied. As the pH of the suspending buffer approaches the isoelectric point of the virus, eq 7, or any simple static theory relating mobilities to charges, is not applicable because of time fluctuations in the charge density. For this reason, Table I contains no charge density values below pH 5. Table I also includes our measured mobility and the charge density (from eq 7a) for human erythrocytes and, for comparison, data from the literature for normal and transformed hamster fibroblasts (Ambrose, 1966). The most obvious feature of the data is the approximate constancy among these viruses of the mobilities in the high pH region. Thus the data indicate that the mobility measured at pH ≥7 may be a general characteristic of this class of viruses and, in combination with the diffusion constant and the buoyant density, may be useful in assaying for the presence of such viruses. The lack of wide variation among the viruses in surface charge may be an obvious consequence of the fact that the virus envelope is derived from the host cellular membrane (Bentvelzen, 1974), and that all animal membranes have about the same surface charge density. A comparison between the virus and erythrocyte data at pH >7 indicates that, in terms of the surface charge density, the envelope of the RNA tumor virus is not very different from the erythrocyte membrane. The surface charge density of transformed hamster fibroblasts, calculated from the data in Ambrose (1966), is about 80% higher than that of the viruses. However, there is no ionic strength dependence of the mobilities for these cells reported in the literature, thus the applicability of the data analysis to these cells cannot be ascertained, and a discussion of these quantitative differences between virus and fibroblast surfaces is inadvisable.

From this discussion, we also conclude that in order to measure surface charge densities, or in order to distinguish among components in a mixed system strictly by their surface charge densities, the electrophoretic measurements should be performed at high ionic strength (i.e., $\kappa R \gg 1$). The use of low ionic strength solvents enhances the geometric contribution to mobility which might be helpful if mobilities are the basis for detecting specific particles from background components.

Acknowledgments

We acknowledge the collaboration of Dr. D. Gill in the early stages of this work, helpful discussions with Dr. T. Kushida throughout the research, and we thank Mr. Ernest Retzel for technical assistance with part of this work.

References

Ambrose, E. J. (1966), *Prog. Biophys. Mol. Biol. 16,* 243-265.

Bader, J. P. (1969), in The Biochemistry of Viruses, Levy, H. B., Ed., New York, N.Y., Marcel Dekker, pp 293-327.

Bennett, A. J., and Uzgiris, E. E. (1973), *Phys. Rev. A 8,* 2662-2669.

Bentvelzen, P. (1974), in Viruses, Evolution and Cancer, Kurstak, E., and Maramorosch, K., Ed., New York, N.Y., Academic Press, pp 280-367.

Booth, F. (1950), *Proc. R. Soc. London, Ser. A 203,* 514-533.

Born, M., and Wolf, E. (1964), Principles of Optics, New York, N.Y., Macmillan.

Clark, N. A., Lunacek, J. H., and Benedek, G. B. (1970), *Am. J. Phys. 38,* 575-585.

Dodge, J. T., Mitchell, C., and Hanahan, D. J. (1963), *Arch. Biochem. Biophys. 100,* 119-130.

Heard, D. H., and Seaman, G. V. F. (1960), *J. Gen. Phys. 43,* 635-645.

Henry, C. H. (1931), *Proc. R. Soc. London, Ser. A 133,* 106-129.

Hill, B. J., Baxby, D., and Douglas, H. W. (1972), *J. Gen. Virol. 16,* 39-46.

Long, C. (1961), The Biochemist's Handbook, Princeton, N.J., Van Nostrand.

Luftig, R., and Kilham, S. S. (1971), *Virology 46,* 277-297.

Luftig, R. B., McMillan, P. N., Culbreth, K., and Bolognesi, D. P. (1974), *Cancer Res. 34,* 1694-1706.

Lyons, M. J., and Moore, D. H. (1965), *J. Natl. Cancer Inst. 35,* 549-565.

Manning, J. S., Hackett, A. J., Cardiff, R. D., Mel, H. C., and Blair, P. B. (1970), *Virology 40,* 912-919.

Moore, D. H., and Lyons, M. J. (1963), *J. Natl. Cancer Inst. 31,* 1255-1273.

Mora, P. T., McFarland, V. W., and Luborsky, S. W. (1966), *Proc. Natl. Acad. Sci. U.S.A. 55,* 438-445.

Pusey, P. N., Koppel, D. E., Schaefer, D. W., Camerini Otero, R. D., and Koenig, S. H., (1974), *Biochemistry 13,* 952-960.

Rimai, L., Hickmott, J. T., Cole, T., and Carew, E. B., (1970), *Biophys. J. 10,* 20-37.

Salmeen, I., Rimai, L., Liebes, L., Rich, M. A., and McCormick, J. J., (1975), *Biochemistry 14,* 134-141.

Sarkar, N. H., Moore, D. H., and Charney, J. (1973), *Cancer Res. 33,* 2283-2290.

Schaffer, F. L., and Fromhagen, L. H. (1965), *Virology 25,* 662-664.

Sharp, D. G., and Beard, J. W. (1954), *Biochim. Biophys. Acta 14,* 12-17.

Tanford, C. (1961), Physical Chemistry of Macromolecules, New York, N.Y., Wiley.
Uzgiris, E. E. (1972), *Opt. Commun. 6,* 55–57.
Uzgiris, E. E. (1974), *Rev. Sci. Instrum. 45,* 74–80.
Uzgiris, E. E., and Costaschuk, F. M. (1973), *Nature (London), Phys. Sci. 242,* 77–79.
Uzgiris, E. E., and Kaplan, J. H. (1974), *Anal. Biochem. 60,* 455–461.
Ware, B. R., and Flygare, W. H. (1971), *Chem. Phys. Lett. 12,* 81–85.

Evidence for Photoinduced Cross-Linkage, in Situ, of 30S Ribosomal Proteins to 16S rRNA†

Lester Gorelic

ABSTRACT: The effects of ultraviolet radiation on the 30S ribosomal subunit of *Escherichia coli* were studied. Irradiation in aqueous solution under anaerobic conditions resulted in a dose-dependent decrease in the separability of the rRNA and protein components of the 30S ribosomal subunit in 4 *M* urea–3 *M* LiCl. The results of gel filtration studies of the irradiated ribosomes before and after treatment with pancreatic ribonuclease indicated that the decrease in separability of the ribosome components was a result of the photoinduced formation of covalent RNA–protein cross-links. The number of covalent cross-links was estimated to correspond to less than 3 per 10,000 daltons of ribosomal proteins. One-dimensional gel electrophoresis studies of the course of the photoinduced cross-linkage reaction indicated that cross-linkage of individual 30S ribosomal proteins to the 16S rRNA proceeds in two dose-dependent steps. The first step requires an input of 1×10^{20} quanta of 253.7-nm radiation and results in the cross-linkage of at least five ribosomal proteins to the 16S rRNA. The second step requires a total input of 2×10^{20} quanta of 253.7-nm radiation, and results in the cross-linkage of most of the remaining 30S ribosomal proteins to the 16S rRNA.

Ultraviolet irradiation of stable complexes between proteins and nucleic acids results in the covalent cross-linkage of the proteins to the nucleic acid molecules (Markovitz, 1972; Lin and Riggs, 1974; Schoemaker and Schimmel, 1974; Strniste and Smith, 1974). Since it has been shown that several ribosomal proteins can interact directly with the rRNA components of the ribosomal subunits (Schaup et al., 1970,1971; Gray et al., 1973a,b; Yug and Wittmann, 1973; Garrett et al., 1974; Zimmermann et al., 1974), it is reasonable to expect that ultraviolet (uv) irradiation of the individual ribosomal subunits or of the intact 70S ribosome complex would result in some nucleic acid–protein cross-linkage.

The formation of an RNA–protein cross-link in irradiated ribosomes requires that a ground-state or photoexcited protein molecule be sufficiently close to the heterocyclic rings of a photoexcited or ground-state rRNA base, respectively, to form a stable covalent bond. Consequently, the pattern of photoinduced protein–nucleic acid cross-linkage in the individual ribosomal subunits or in the 70S complex could provide valuable information concerning the relative contribution of direct interactions between the rRNA bases and various ribosomal proteins to ribosome structure. It is also possible that a study of photoinduced protein–nucleic acid cross-linkage in the individual ribosomal subunits may provide an explanation for the known photoinactivation of the functional activity of the ribosomal subunits (Kagawa et al., 1967; Tokimatsu et al., 1968; Yasuda and Fukutome, 1970).

For these reasons, a detailed investigation of the photochemistry of the *Escherichia coli* ribosomal subunits was undertaken. In previous reports (Gorelic, 1974,1975) it was demonstrated that uv irradiation of intact 50S ribosomal subunits resulted in the covalent cross-linkage of specific 50S ribosomal proteins to the rRNA components of the subunit. The data presented in this report indicate that photoinduced covalent cross-linkage of specific ribosomal proteins to rRNA also occurs in irradiated 30S subunits.

Experimental Section

Materials. Pancreatic ribonuclease was obtained from Worthington Biochemicals. Ribonuclease-free deoxyribonuclease I used in the preparation of cell-free extracts of *E. coli* was obtained from Worthington Biochemicals. Ribonuclease-free sucrose was obtained from Schwarz/Mann. Acrylamide and bismethyleneacrylamide were obtained from Eastman Kodak and were recrystallized before use. *N,N,N′,N′*-Tetramethylenediamine was obtained from Eastman Kodak and was distilled over zinc dust in a nitrogen atmosphere and stored over KOH pellets. Sephadex G-100 was obtained from Pharmacia. Bio-Gel A-5.0m was obtained from Bio-Rad Laboratories. Potassium ferrioxalate was prepared by a published procedure (Hatchard and Parker, 1956). Oxygen-free nitrogen was obtained from the Linde Corporation. All other reagents were Analytical Reagent grade.

Ribosomal subunits (30 S and 50 S) were prepared and isolated according to previously published procedures (Tiss-

† From the Department of Chemistry, Wayne State University, Detroit, Michigan 48202. *Received May 15, 1975.* This work was supported by a grant from the Research Corporation, Wayne State University Faculty Research Award, Grant No. CA 18046 from the National Institutes of Health, and U.S. Public Health Service Career Development Award No. CA 70999.